Inorganic Chemistry

Article

pubs.acs.org/IC

Halide Free $M(BH_4)_2$ (M = Sr, Ba, and Eu) Synthesis, Structure, and Decomposition

Manish Sharma,[†] Emilie Didelot,[‡] Alexandra Spyratou,[†] Latévi Max Lawson Daku,[†] Radovan Černý,*[,‡] and Hans Hagemann*[,†]

[†]Department of Physical Chemistry, University of Geneva, 30, quai Ernest-Ansermet, CH1211 Geneva 4, Switzerland

[‡]Laboratory of Crystallography, Department of Quantum Matter Physics, University of Geneva, 24, quai Ernest-Ansermet, CH1211 Geneva 4, Switzerland

Supporting Information

ABSTRACT: Borohydrides have attained high interest in the past few years due to their high volumetric and gravimetric hydrogen content. Synthesis of di/trimetallic borohydride is a way to alter the thermodynamics of hydrogen release from borohydrides. Previously reported preparations of $M(BH_4)_2$ involved chloride containing species such as $SrCl_2$. The presence of residual chloride (or other halide) ions in borohydrides may change their thermodynamic behavior and their decomposition pathway. Pure monometallic borohydrides are needed to study decomposition products without interference from halide impurities. They can also be used as precursors for synthesizing di/trimetallic borohydrides. In this paper we present a way to synthesize halide free alkaline earth metal (Sr, Ba) and europium borohydrides starting with the respective hydrides as precursors. Two novel high temperature polymorphs of Sr and Eu borohydrides and four polymorphs of Ba borohydride have been characterized by synchrotron X-ray powder diffraction, thermal analysis, and Raman and infrared spectroscopy and supported by periodic DFT calculations. The decomposition routes of these borohydrides have also been investigated. In the case of the decomposition of strontium and europium borohydrides, the metal borohydride hydride ($M(BH_4)H_3$, M = Sr, Eu) is observed and characterized. Periodic DFT calculations performed on room temperature $Ba(BH_4)_2$ revealed the presence of bidentate and tridentate borohydrides.

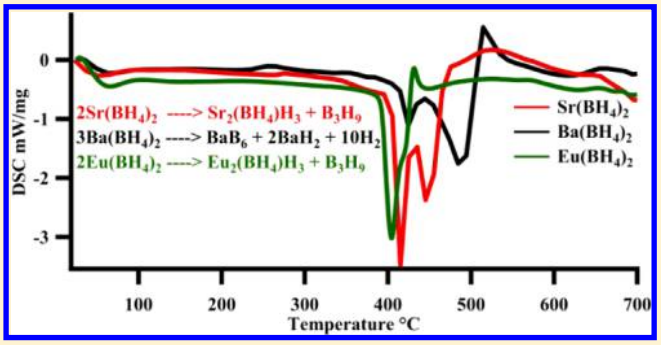

INTRODUCTION

Metal borohydrides are materials of great interest due to their high gravimetric and volumetric content of hydrogen, but the challenge lies in designing a system which can release hydrogen safely and reversibly at suitable temperature and pressure.[1,2] Synthesis of di/trimetallic borohydrides, anion exchange, and nanoconfinement are some ways to improve the kinetics and thermodynamics of hydrogen release.[3,4] A second field of metal borohydride application which developed recently is situated in batteries where they play the role of solid state electrolytes due to the high mobility of cations like Li^+ or Na^+ in certain borohydrides[5,6] or other mixed-anion hydroborates.[7] Rare earth containing borohydrides have also interesting luminescence and magnetic properties.[8,9]

Monometallic borohydrides may be used as precursors for synthesizing bi- or trimetallic borohydrides. For example, $Sr(BH_4)_2$ and $Eu(BH_4)_2$ are used for heterovalent doping in recently discovered garnet-borohydrides and Li^+ conductors, and $Eu(BH_4)_2$ is of interest for luminescent perovskite-borohydrides.[8,10] They are often synthesized via halide containing synthetic routes. Furthermore, anion-substitution $BH_4^- \leftrightarrow X^-$ (X^- = Cl^-, Br^-, I^-) can readily be accommodated in borohydrides. The presence of a halide ion changes the crystal symmetry and physical properties like melting point and hydrogen release temperature.[11−16] With F^- ions being much smaller than BH_4^-, they can substitute for H^- in BH_4^- resulting in $BH_xF_{(4-x)}^-$ ions.[17,18] This again changes the chemical and physical properties of borohydrides due to a change in bond strength arising from substitution of H^- with highly electronegative F^- ions.[19,20]

The synthesis of metal borohydrides is carried out either by mechanochemical processes such as ball milling or by wet chemistry.[21] Ball milling reactions can be adjusted by controlling factors like milling time, cooling breaks during the milling, milling frequency, vial and ball composition and size, powder to ball weight ratio, milling atmosphere, and pressure of the gas selected for milling.[22] Although ball milling appears to be a simple technique to produce a large variety of borohydrides, undesired products may also be formed as a result of various competing reactions occurring simultaneously.[22−24] For example, $LiZn_2(BH_4)_5$ is formed rather than $Zn(BH_4)_2$ when $LiBH_4$ is milled with $ZnCl_2$; the presence of

Received: April 23, 2016
Published: June 28, 2016

DOI: 10.1021/acs.inorgchem.6b00931
Inorg. Chem. 2016, 55, 7090−7097

chloride impurities may form mixed-anion compounds, as solid solutions of $LiBH_4$ with other lithium halides are formed.[25−28]

Exchange reactions in solution can be one of the approaches to synthesize borohydrides. In general, Na/Li borohydride is reacted with a metal halide to form metal borohydride with sodium/lithium chloride as a side product. For example, $NaBH_4$ when reacted with LiX (X = Cl, Br, I) in isopropylamine gives $LiBH_4$.[29] A $LiBH_4$ and $MgCl_2$ mixture in diethyl ether gives $Mg(BH_4)_2$, and $LiBH_4$ with $MnCl_2$ in toluene−dimethylsulfide gives $Mn(BH_4)_2$. $LiBH_4$ with $AlCl_3$ in toluene forms $Al(BH_4)_3$. LiCl is a side product in each case.[30−33]

Several synthesis schemes of $Eu(BH_4)_2$ were reported recently.[34,35] Humphries et al. synthesized $Eu(BH_4)_2$ from $EuCl_3$ and $LiBH_4$ in diethyl ether, and the product was washed with dimethyl sulfide to remove LiCl.[35] The crystal structure and synthesis of $Sr(BH_4)_2$ via metathesis reaction between $LiBH_4$ and $SrCl_2$ was also reported recently.[36] Similarly, $Ba(BH_4)_2$ was prepared by a chloride containing synthetic route.[37] While an α-PbO_2 type polymorph has been reported as ambient structure for $Sr(BH_4)_2$ and $Eu(BH_4)_2$,[34−36] two polymorphs isostructural to their chloride analogues have been reported for $Ba(BH_4)_2$.[37]

In this paper we present a way to synthesize halide free strontium, barium, and europium borohydrides starting with their respective hydrides as precursor. The crystal structures of several polymorphs are characterized and put into a context of crystal chemistry of homoleptic metal borohydrides. Metal borohydride hydrides are reported as a first decomposition intermediate in europium and strontium borohydride.

EXPERIMENTAL SECTION

Synthesis of $M(BH_4)_2$ (M = Sr, Ba, Eu). The successful synthesis scheme is similar to the $Mg(BH_4)_2$ synthesis reported by Chlopek et al.[38] MH_2 is activated by ball milling under inert conditions (Ar atmosphere, 12 cycles, 600 rpm for 6 min each with a pause of 2 min). Freshly ball milled MH_2 is mixed in excess (of stoichiometric amount, Table 1) of triethyl amine borane. This mixture is heated overnight under reflux at a temperature of 100 °C and then at a temperature of 145 °C for 5 h.

Table 1. Sample Prepared by Reaction of Premilled Hydride with Triethyl Amine Borane

	hydride			
sample	gram	mmol	triethylamine borane	product
S1	SrH_2, 0.5	5.5	1.7 mL, 11.5 mmol	$Sr(BH_4)_2$
S2	BaH_2, 0.5	3.6	1.1 mL, 7.5 mmol	$Ba(BH_4)_2$
S3	EuH_2, 0.6	3.9	1.2 mL, 8.1 mmol	$Eu(BH_4)_2$

$$MH_2 + 2(C_2H_5)_3N{-}BH_3 \rightarrow M(BH_4)_2 + 2N(C_2H_5)_3$$

In the case of EuH_2, a change in sample color from dark red to white can also be observed. The mixture is cooled down to room temperature and is washed with cyclohexane. The residue is dried under dynamic vacuum up to the temperature of 100 °C for a few hours. The solid product was periodically analyzed with IR spectroscopy to monitor the presence of residual solvent.

All the starting materials were commercially available. EuH_2 was kindly provided by Dr. Holger Kohlmann.

Laboratory X-ray Powder Diffraction (XPD). XPD patterns for preliminary analysis were obtained on a STOE STADI-P diffractometer in Debye−Scherrer geometry with monochromated Cu Kα1 radiation.

Synchrotron Radiation X-ray Powder Diffraction (SR-XPD). Data used for crystal structure solution and refinements in this study were collected between room temperature (RT) and 773 K at the Swiss-Norwegian Beamlines of ESRF (European Synchrotron Radiation Facility, Grenoble, France). The data was measured on a Dectris Pilatus M2 detector at a wavelength of 0.81710(1) and 0.81984(1) Å. The temperature was controlled with the Oxford Cryostream 700+ or hot air blower, and the 2-dimensional images were integrated and treated with FIT2D.[39] For all measurements the samples were loaded into borosilicate capillaries of diameter 0.5 mm, which were spun during data acquisition. The wavelength was calibrated using the external NIST SRM660b LaB_6 standard.

FTIR and Raman. Temperature dependent FTIR experiments on solid samples were performed with a Biorad Excalibur Instrument equipped with a Specac Golden Gate heatable ATR setup. The spectral resolution was set to 1 cm^{-1}. The sample was heated in steps to 280 °C (from room temperature) and then cooled down to room temperature.

Raman spectra were measured using 488 nm excitation and a Kaiser Optical Holospec monochromator equipped with a liquid nitrogen cooled CCD camera.

Thermal Analysis (DSC). Differential scanning calorimetry data were measured using a NETZSCH STA449 F3 instrument. The measurements were performed under an inert atmosphere of nitrogen with a purge rate of 20 mL/min. The samples were contained in Al_2O_3 crucibles with a lid to prevent exposure to atmosphere while mounting. Heating rate was 10 °C/min.

CALCULATIONS

Crystal Structure Solution. Indexing the powder patterns of individual phases is possible thanks to "decomposition-aided indexing" by means of temperature ramp,[40] i.e., separating the peaks of individual phases by correlating them to their temperature dependent vanishing from the diffraction pattern. After assigning peaks this way, indexing of each novel phase was tempted on the basis of 10−15 peaks with the dichotomy routine implemented in Fox.[41] The correct indexing was selected not only according to the highest figure of merit as implemented in each indexing program, but also according to systematic extinctions, obtained by a careful visual inspection of powder patterns, which should be crystallographic, i.e., corresponding to crystallographic space groups. Structure solution was always attempted in the highest symmetry space group compatible with the extinction symbol. The structures were modeled with Sr, Ba, and Eu, as free atoms and BH_4 groups as rigid bodies with fixed B−H distances (1.13 Å), and solved in direct space using Fox. Selected structural models were refined with FullProf,[42] treating the BH_4 tetrahedra as semirigid bodies with a constrained ideal tetrahedral angle and B−H distances, constrained to adopt a value of 1.13 Å. All resulting structural models were checked with the ADDSYM routine implemented in the PLATON software.[43] The crystal structure of $o1$-$Ba(BH_4)_2$ was also treated with postexperiment DFT optimizations.

DFT. Density functional theory[44,45] was applied to the characterization of the structural and vibrational properties of three working models for $Ba(BH_4)_2$ structure. Periodic DFT calculations were thus performed with the PBE functional[46] using the Quantum Espresso program package (version v.5.1), which is based on pseudopotentials and planewaves.[47] The calculations consisted of geometry optimizations followed by the determination of the phonons at Γ within density functional perturbation theory.[48] We employed ultrasoft pseudopotentials[49] and a 5 × 4 × 4 Monkhorst−Pack grid,[50] and expanded the wave functions and the charge density in plane waves up to a kinetic-energy cutoff of 80 and 800 Ry, respectively.

In order to calculate intensities for Raman spectra, additional calculations were performed at the LDA level,[51,52] due to the fact that third order derivatives are not implemented with GGA. These calculations used norm-conserving Trouiller−Martins type pseudopotentials,[53] a planewave cutoff of 160 Ry, and the same 5 × 4 × 4 Monkhorst−Pack grid.

DOI: 10.1021/acs.inorgchem.6b00931
Inorg. Chem. 2016, 55, 7090−7097

RESULTS

Synthesis. The presence of the final product was confirmed by IR spectroscopy using the database of known borohydride IR spectra.[54] Figure 1 shows IR spectra for $M(BH_4)_2$ (M = Eu, Sr, or Ba). These spectra indicate the absence of any solvent or water. Various other methods for synthesis were also tried which resulted in the presence of a large amount of impurities (solvent or starting reagents). These results are discussed in Supporting Information.

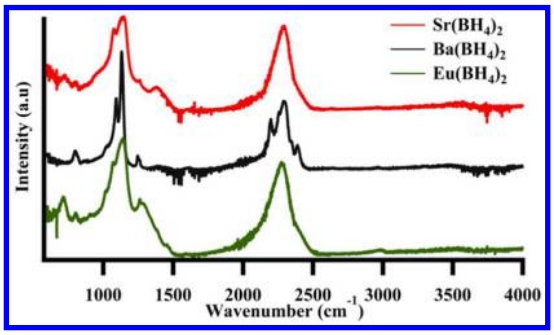

Figure 1. IR spectra of freshly synthesized $Sr(BH_4)_2$ (upper, sample S1), $Ba(BH_4)_2$ (middle, sample S2), and $Eu(BH_4)_2$ (lower, sample S3).

Phase Analysis by SR-XPD and DSC. The initial analysis of the samples has been done by combining temperature dependent synchrotron radiation X-ray powder diffraction (SR-XPD) and DSC. Eight new compounds and two known from previous works[35,36] were identified in the samples. The lattice parameters, space groups and relevant structural prototypes of compounds presented in this section are summarized in Table 2 explaining also the abbreviation used in the names of compounds. The temperature dependent SR-XPD data also showing phase composition is given in Figures 2 and 4 and Figure S1, and the corresponding DSC data is presented in Figure 3. Rietveld plot for selected powder patterns are given in Supporting Information (Figures S2–S10).

Europium and Strontium Borohydrides. Only one crystalline phase is present in the as-synthesized samples S3 and S1, which was identified as *o*-$Eu(BH_4)_2$and *o*-$Sr(BH_4)_2$ in agreement with refs 35 and 36.

Both compounds transform on heating into isostructural *t*-$Eu(BH_4)_2$ (395 °C) and *t*-$Sr(BH_4)_2$ (450 °C). Note the much higher thermal stability of the orthorhombic polymorph compared to chloride containing mixtures studied in refs 35 and 36. The tetragonal polymorph is visible up to 425 °C for $Eu(BH_4)_2$ where the sample melts, and up to 490 °C for $Sr(BH_4)_2$ where its diffraction peaks disappear, but the sample does not melt up to 500 °C, the highest temperature in our experiment. The peaks of a cubic polymorph were also observed appearing and disappearing at the same temperatures as the tetragonal polymorph in both samples. The coexistence

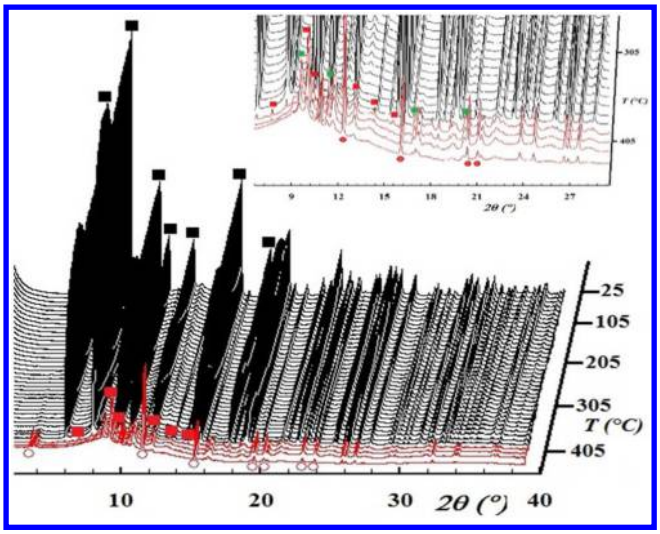

Figure 2. Powder diffraction patterns as a function of temperature (T-ramp) for $Eu(BH_4)_2$ (sample S3, heating rate of 10 °C/min, λ = 0.8171 Å) with black square *o*-$Eu(BH_4)_2$, red square *t*-$Eu(BH_4)_2$, and empty red circle $Eu_2(BH_4)H_3$; zoom: green square *c*-$Eu(BH_4)_2$.

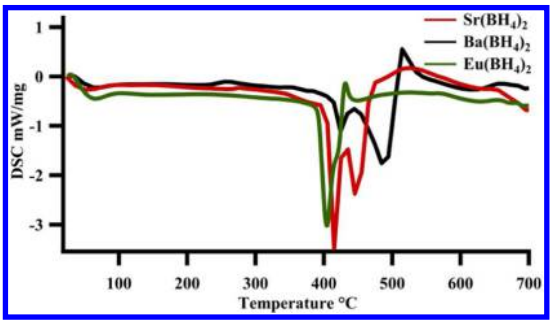

Figure 3. DSC heating curves for $Sr(BH_4)_2$ (sample S1), $Ba(BH_4)_2$ (sample S2), and $Eu(BH_4)_2$ (sample S3).

Table 2. Compounds Observed in the Three Synthesized Samples[a]

sample	compd	symmetry	Z	prototype	obsd within [°C]	V [Å^3]	a [Å]	b [Å]	c [Å]	T [°C]
S1	*o*-$Sr(BH_4)_2$	*Pbcn*	4	*α*-PbO_2	25–450	449.17(5)	7.0080(4)	8.4458(5)	7.5888(4)	70
	t-$Sr(BH_4)_2$	$P4_12_12$	4	*ht*-ZrO_2	450–490	344.07(20)	5.4208(15)		11.709(5)	490
	c-$Sr(BH_4)_2$	$Fm\bar{3}m$	4	CaF_2	450–500	359.22888	7.10870			490
S2	*o*1-$Ba(BH_4)_2$	*Pnnm*	2	$CaCl_2$	25–395	244.838(9)	6.98476(15)	7.22841(16)	4.84936(10)	210
	*o*2-$Ba(BH_4)_2$	*Pbcn*	4	*α*-PbO_2	395–445	528.56(3)	7.4043(2)	8.0935(2)	8.8201(3)	430
	t-$Ba(BH_4)_2$	$P4_12_12$	4	*ht*-ZrO_2	445–500	391.54(5)	5.5805(4)		12.5727(9)	500
	c-$Ba(BH_4)_2$	$Fm\bar{3}m$	4	CaF_2	460–500	356.85(9)	7.0930(11)			500
S3	*o*-$Eu(BH_4)_2$	*Pbcn*	4	*α*-PbO_2	25–395	456.34(2)	7.0205(2)	7.62211(20)	8.5281(2)	235
	t-$Eu(BH_4)_2$	$P4_12_12$	4	*ht*-ZrO_2	395–425	339.99(7)	5.4091(6)		11.6201(17)	395
	c-$Eu(BH_4)_2$	$Fm\bar{3}m$	4	CaF_2	395–425	351.93(15)	7.0602(17)			395

[a]Temperature range of observation, space group, structural prototype, and lattice parameters from Rietveld refinements at given temperature (unit cell parameters with s.u. are from Rietveld refinement). The meaning of the prefix in the compound name: *o*- for orthorhombic, *t*- for tetragonal, and *c*- for cubic.

DOI: 10.1021/acs.inorgchem.6b00931
Inorg. Chem. 2016, 55, 7090–7097

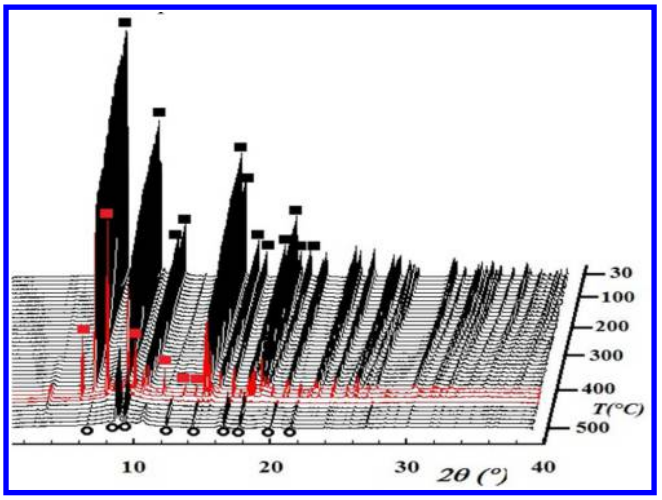

Figure 4. Powder diffraction patterns as a function of temperature (T-ramp) for $Ba(BH_4)_2$ (sample S2, heating rate of 10 °C/min, λ = 0.81984 Å) with black square *o*1-$Ba(BH_4)_2$, red square *o*2-$Ba(BH_4)_2$, and empty circle *t*-$Ba(BH_4)_2$.

of both, tetragonal and cubic, polymorphs points to a displacement phase transition between them (see the structural relation discussed below), and second order phase transition.

The thermal decomposition route in both samples is rather complex as already observed in refs 35 and 36. It involves several unidentified crystalline phases. As a main decomposition product, a trigonal ($P\bar{3}m1$) borohydride−hydride $M_2(BH_4)H_3$ was observed from 395 °C for $Eu(BH_4)_2$, and from 410 °C for $Sr(BH_4)_2$. While $Sr_2(BH_4)H_3$ is stable at least up to 500 °C where the diffraction peaks of SrH_2 (*Pnma*) start to grow, $Eu_2(BH_4)H_3$ melts in the multiphase sample S3 at 425 °C, and recrystallizes on cooling.

The initial thermal decomposition of $Eu(BH_4)_2$ and $Sr(BH_4)_2$ can be therefore simplified as

$$2M(BH_4)_2 \rightarrow M_2(BH_4)H_3 + B_3H_9$$

The decomposition is rather slow, as our dynamic heating experiment with the heating rate of 10 °C/min contains coexistence of the borohydride (which even shows polymorphic transformation) and its decomposition product, the borohydride−hydride. It is therefore very probable that the tetragonal and cubic polymorphs of $M(BH_4)_2$ are metastable in both systems.

The B_3H_9 decomposition product can be understood as a higher borane anion like $B_{12}H_{12}$ and released hydrogen or as a diborane B_2H_6. As the ratio M/B is higher in the borohydride−hydride $M_2(BH_4)H_3$, it is not probable that metallic closoboranes or other salts containing higher boranes anions are formed. Rather, the diborane is formed during the thermal decomposition followed by the decomposition of the diborane at temperatures higher than ∼300 °C.

The DSC curves of samples S1 and S3 show on heating the first strong endothermic peak which corresponds to the decomposition of the borohydride in both samples (Figure 3). The second endothermic peak, better resolved in $Sr(BH_4)_2$, corresponds to the decomposition of the borohydride−hydride in this sample and to the melting in $Eu(BH_4)_2$.

Barium Borohydride. A new polymorph *o*1-$Ba(BH_4)_2$ is present in as-synthesized sample S2. This polymorph is not observed in Eu- and Sr-borohydrides. On heating, the *o*1-$Ba(BH_4)_2$ transforms at 395 °C into the *o*2-$Ba(BH_4)_2$ polymorph, isostructural to the orthorhombic polymorph in Eu- and Sr-borohydrides. At 445 °C it transforms into the *t*-$Ba(BH_4)_2$ polymorph, known already from two other systems. At 460 °C the cubic polymorph also appears. On cooling down to RT the tetragonal and cubic polymorphs with 8-fold coordination of Ba^{2+} (see below) do not transform to the orthorhombic polymorphs with octahedral coordination, which is probably due to slow kinetics as the cooling was rather fast (20 °C/min). Polymorphs with higher coordination number of 9 were observed only in chloride based synthesis following the structure types of the two $BaCl_2$ polymorphs.[37]

Chloride free $Ba(BH_4)_2$ is stable at least up to 500 °C, the highest temperature in our experiment. Several unexplained diffraction peaks were observed in T-ramps, but seem not to be related to $Ba(BH_4)_2$ decomposition, and may belong to residual impurities from the synthesis.

DSC heating trace for $Ba(BH_4)_2$ (shown in Figure 3) presents two endothermic peaks around 400 and 450 °C, in agreement with structural phase transitions observed by X-ray diffraction.

Heating $Ba(BH_4)_2$ ex situ up to 750 °C leads to the formation of BaB_6 along with two unidentified phases (Figure S11 in Supporting Information).

Tentatively, the decomposition of $Ba(BH_4)_2$ can be described as

$$3Ba(BH_4)_2 \rightarrow BaB_6 + 12H_2 + 2Ba$$

or

$$3Ba(BH_4)_2 \rightarrow BaB_6 + 2BaH_2 + 10H_2$$

As the B/Ba ratio in BaB_6 is higher than in $Ba(BH_4)_2$, it seems unlikely that boron would be present in other decomposition products. It is possible that during our experiments the metallic Ba reacted with the container to yield the unknown phases observed.

Vibrational Spectroscopy. IR spectra shown in Figure 1 are typical for isolated BH_4^- ions in the solid.[54] No strong splitting of the B−H stretching mode as observed[13,24,28] for $Sc(BH_4)_4^-$ is seen. Some weak additional bands below 1000 cm^{-1} and underlying B−H deformation modes from 1000 to 1400 cm^{-1} are probably related to borate species present as impurities.

The temperature dependent IR spectra up to 280 °C did not reveal any structural changes of the $M(BH_4)_2$ samples in agreement with the X-ray and DSC measurements reported above. This behavior is illustrated for $Eu(BH_4)_2$ in Figure 5 and in SI for $Sr(BH_4)_2$ and $Ba(BH_4)_2$ (Figures S12 and S13).

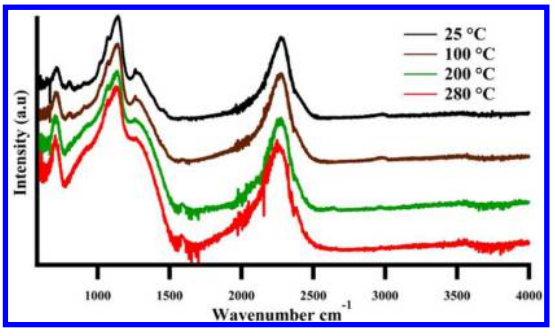

Figure 5. IR spectra as a function of temperature for $Eu(BH_4)_2$, sample S3.

DOI: 10.1021/acs.inorgchem.6b00931
Inorg. Chem. 2016, 55, 7090−7097

DISCUSSION

Synthesis. In order to synthesize solvent free $Ba(BH_4)_2$, the product obtained after the reaction of BaH_2 with triethyl amine was divided into two parts. The first part was subjected to dynamic heating under vacuum which gave pure $Ba(BH_4)_2$ as shown in Figure 1 and Figure S13. The second part was dissolved in water to wash the organic solvent attached to it. It was observed that $Ba(BH_4)_2$ is stable in water and can be recrystallized to form $Ba(BH_4)_2$ (Figure 6) with trace amounts

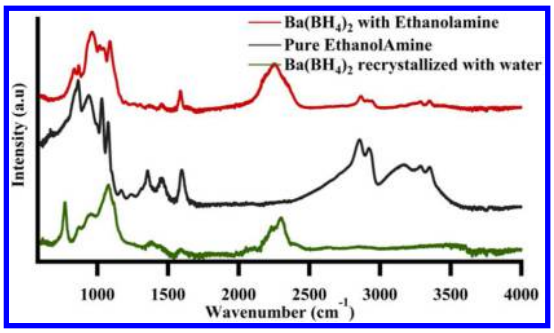

Figure 6. IR spectra of $Ba(BH_4)_2$ recrystallized from water.

of water. O−H and N−H stretching bands are observed above 3000 cm^{-1}, and the NH_2 or OH_2 deformation bands around 1598 and 1630 cm^{-1}, respectively. There is a possibility of partial hydrolysis leading to a formation of borate, which brings the difference in spectra close to 1000 wavenumbers (green curve in Figure 6).

Photoluminescence. Divalent Eu ions in solids find many applications for luminescent materials. As borohydrides are inherently reducing materials, one does not expect to observe Eu^{3+} ions, as one can for instance in Eu-doped oxides. The luminescence of Eu^{2+} in the perovskites[8] $CsEu(BH_4)_3$ and Eu-doped $CsCa(BH_4)_3$ was observed at 485 nm at room temperature. The excitation and emission spectra of $Eu(BH_4)_2$ have been briefly shown previously.[8] There is a single emission band at 463 nm (fwhm 55 nm), corresponding to the CIE color coordinates $x = 0.145$, $y = 0.134$ (Figure S19). The Stokes shift (0.25 eV) is typical for a normal f−d transition of Eu^{2+}.[55] Thus, the emission can already be excited at 400−410 nm, which could make $Eu(BH_4)_2$ or Eu-doped $Sr(BH_4)_2$ useful blue phosphors for trichromatic light sources.

Crystal Structures. Three different polymorphs of $M(BH_4)_2$, and one decomposition product, borohydride−hydride $M_2(BH_4)H_3$, have been observed in the samples S1−S3 (Table 2). Their structures and structural prototypes are discussed in this section. Interatomic distances and angles for each phase can be found in CIF files resulting from Rietveld refinement (DFT results are used instead for *o*1-$Ba(BH_4)_2$) and submitted as Supporting Information. Similar ionic radii of 6-fold coordinated cations[56] Sr^{2+} (1.32 Å) and Eu^{2+} (1.31 Å) explain the structural similarity of borohydrides and borohydride−hydride of these two cations. Bigger Ba^{2+} (1.49 Å) crystallizes in similar structural prototypes, but in another prototype for the ambient phase.

The borohydride coordination mode and intermolecular H−H contacts are also discussed in the next section using the DFT optimized structure of *o*1-$Ba(BH_4)_2$.

***o*1-$Ba(BH_4)_2$.** $Ba(BH_4)_2$ was synthesized as *Pnnm* polymorph ($CaCl_2$ structure type) which is an orthorhombic deformation of the tetragonal rutile type (see Figure 7). The latter is the prototype of β-$Ca(BH_4)_2$, and the former may be stabilized at higher temperatures by partial borohydride substitution with iodide as was done in $Ca(BH_4)_{1.28}I_{0.72}$.[57]

In order to confirm the space group of $Ba(BH_4)_2$, variable-cell and fixed-cell optimizations were performed in the three candidate space groups, namely, *Immm*, *Imm*2, and *Pnnm*. Phonon calculations were performed after structure optimization. For the first two settings, more than three imaginary frequencies were obtained, while none was obtained for *Pnnm*. Moreover, $Ba(BH_4)_2$ in the *Pnnm* space group is found to be energetically more stable than the other two (*Imm*2 by 30.9 kJ/mol and *Immm* by 42.6 kJ/mol).

For $Ba(BH_4)_2$ in the *Pnnm* space group, two types of structural relaxation were carried out. First, the atomic positions were optimized with the cell parameters kept fixed to their experimental values. In the second type of optimization, both the cell parameters and the atomic positions were relaxed (variable-cell optimization). The relaxation of the cell parameters led to a 4.5% decrease in the volume, while the energy decreased by 4.6 kJ/mol. Figure 8 compares

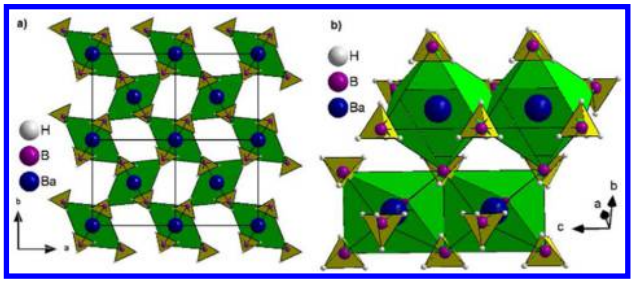

Figure 7. View of *o*1-$Ba(BH_4)_2$, *Pnnm*, $CaCl_2$ structure type, (a) along the *c*-axis, and (b) octahedra sharing corners and edges.

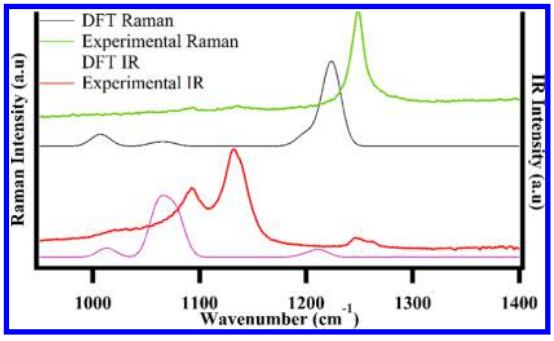

Figure 8. Vibrational spectra (Raman on top and IR on bottom) of $Ba(BH_4)_2$ compared with calculated vibrational spectra for the *Pnnm* structure.

experimental and theoretical results for both IR and Raman spectroscopy for the bending mode region between 1000 and 1400 cm^{-1}. The calculated frequencies of the bending modes are systematically lower than the experimental values, but the splitting is similar, and the relative intensities agree quite well between DFT and experiment. The stretching modes are subject to strong Fermi resonances as observed and analyzed previously for the alkali borohydrides.[58] The complete experimental spectra (from 900 to 2700 cm^{-1}) and a list of calculated frequencies are given in the Supporting Information (Figure S20 and Table ST1). As all 4 B−H bond lengths are very similar, we have applied the GF method to calculate the splitting of the deformation modes using the bond angles from the optimized DFT structure.[59] The ν_2 deformation modes are

DOI: 10.1021/acs.inorgchem.6b00931
Inorg. Chem. 2016, 55, 7090−7097

split by 10 cm^{-1} compared to about 12 cm^{-1} (as calculated from the average values of the factor split components in Table ST1), and the ν_4 mode is split by 17 and 7 cm^{-1} compared to 36 and 10 cm^{-1} from the periodic DFT calculation. The ratio of this splitting (ca. 3:1) appears to be correct, but the magnitude is not. It is not clear whether this could be due to the slight B−H bond length differences (0.002 Å) or other reasons.

Barium is surrounded in the *Pnnm* polymorph by six BH_4^- units in an octahedral coordination. Each octahedron shares all six vertices and two edges building straight chains along the *c*-axis. Each chain shares vertices with four other chains (Figure 7a,b). The distances Ba−B are 3.09 and 3.18 Å from the DFT optimized structure. Each BH_4^- tetrahedron is surrounded by three Ba atoms in nearly planar triangular coordination.

***o*2-Ba(BH$_4$)$_2$, *o*-Eu(BH$_4$)$_2$, *o*-Sr(BH$_4$)$_2$.** $Sr(BH_4)_2$ and $Eu(BH_4)_2$ were synthesized as *Pbcn* polymorphs (α-PbO_2 structure type) in agreement with results reported from chloride based syntheses,[35,36] and $CaCl_2$ type (rutile-like) $Ba(BH_4)_2$ transforms at 395 °C also into this polymorph. Rutile to α-PbO_2 type is a very well-known transition which may for example be induced in rutile by applying a pressure. It may be described by cation jumps or by a slip in 101 planes in the rutile phase; see, for example, pages 67−70 in ref 60. Similar to the $CaCl_2$ type, the α-PbO_2 type structure is also formed by $M(BH_4)_6$ octahedra sharing all six vertices and two edges building zigzag chains along the *c*-axis (Figure 9a). Each chain is

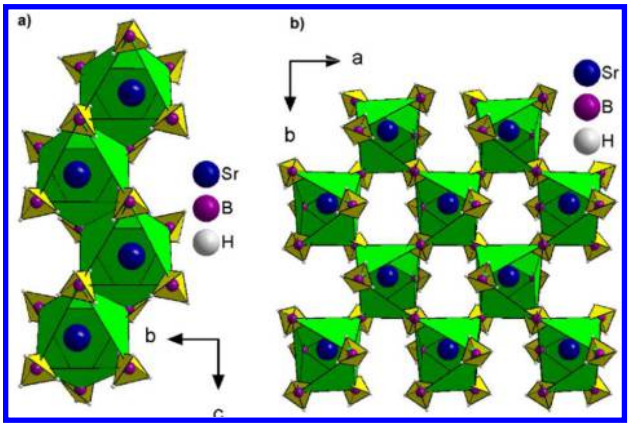

Figure 9. View of *o*-$Sr(BH_4)_2$, *Pbcn*, α-PbO_2 structure type, (a) along the *a*-axis showing octahedral chains running along the *c*-axis, and (b) along the *c*-axis showing the chains interconnected by vertices.

again linked by vertices to four other chains (Figure 9b). The borohydride tetrahedron is surrounded by three M atoms and forms nearly perfect trigonal planar coordination. The Ba−B distances in this polymorph stay between 3.127(6) and 3.289(6) Å, and the Sr−B and Eu−B distances in this polymorph are between 2.961(6) and 3.134(6) Å and between 2.990(6) and 3.096(6) Å, respectively. This structure type is the first high temperature polymorph for $Ba(BH_4)_2$, but it is the room temperature polymorph of $Eu(BH_4)_2$ and $Sr(BH_4)_2$.

***t*-M(BH$_4$)$_2$ (M = Eu, Sr, Ba).** Further heating the α-PbO_2 type polymorph of $Ba(BH_4)_2$ increases its coordination number from 6 to 8, and transforms at 445 °C into the $P4_12_12$ polymorph. This is a noncentrosymmetric superstructure (doubled *c*-axis) of *ht*-ZrO_2 type ($P4_2/nmc$), a deformation of the cubic CaF_2 type which is stabilized by still higher temperatures in ZrO_2, and appears also at higher temperatures in $Ba(BH_4)_2$ (structure not refined). Both Eu and Sr borohydrides also transform on heating into the *ht*-ZrO_2 type polymorph with the appearance of the cubic CaF_2 type polymorph at the highest temperatures (structures not refined).

The M atoms are coordinated in this polymorph by eight BH_4^- (Figure 10a) forming a cube, and each borohydride is

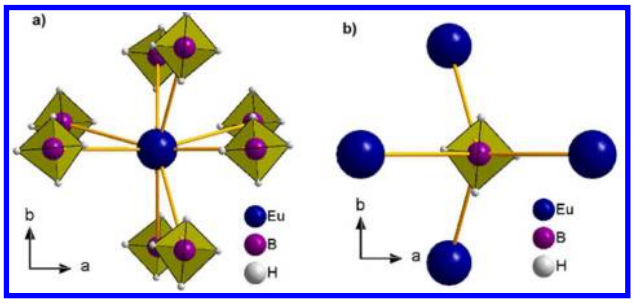

Figure 10. View of *t*-$Eu(BH_4)_2$, $P4_12_12$, superstructure (doubled *c*-axis) of *ht*-ZrO_2 type along the *c*-axis: (a) Eu surrounded by eight BH_4^- units in a cube and (b) tetrahedral coordination of BH_4^- units by Eu atoms.

surrounded by four M atoms in a tetrahedral coordination (Figure 10b). M−B distances are between 3.070(7) and 3.119(8) Å for Eu, 3.0911(7) and 3.1424(7) Å for Sr, and 3.052(4) and 3.499(4) Å for Ba.

M$_2$(BH$_4$)H$_3$ (M = Eu, Sr). This is the main product of thermal decomposition of Eu and Sr borohydrides. The compound is an analogue of halide−hydrides Ca_2BrH_3,[61] Sr_2IH_3,[62] Ba_2IH_3,[63] Ba_2BrH_3, and Ba_2ClH_3,[64] and it is the first compound containing the hydride in two anions, as a simple hydride and as a complex borohydride. Its structure may be described as the *anti* type of $Cd(OH)_2$ (also called brucite or CdI_2) with M on the OH site and BH_4 on the Cd site *stuffed* with H atoms, and is *anti*-isotypic to Li_3LaSb_2 type.[65]

The structure of $M_2(BH_4)H_3$ is built from $(BH_4)M_6$ octahedra sharing six edges with other octahedra and building thus a $Cd(OH)_2$ type layer in the *ab*-plane (Figure 11a). Layers

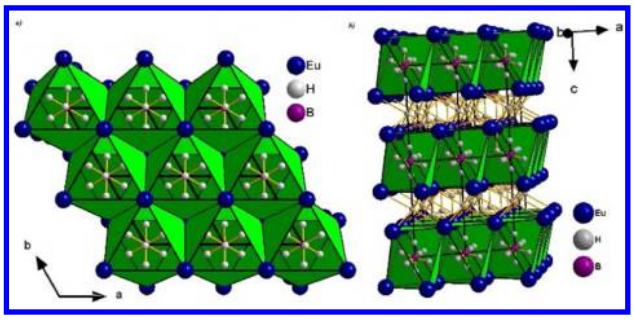

Figure 11. View of $Eu_2(BH_4)H_3$ (a) along the *c*-axis showing the $Cd(OH)_2$ type layer of $(BH_4)Eu_6$ octahedra and (b) along the [$\bar{1}$20] direction showing the stacking of layers and hydrogen positions.

are then simply stacked along the *c*-axis (Figure 11b). Between the layers, H atoms occupy tetrahedral and octahedral sites of the hcp stacking of M atoms. Eu−B distances are 2.849(2) Å, and Sr−B distances are 2.887(3) Å.

Coordination BH$_4$−M. The coordination of cations to borohydride can be discussed in detail only for the *Pnnm* polymorph ($CaCl_2$ structure type) of $Ba(BH_4)_2$ as its structure was optimized by *ab initio* calculation. It is shown in Figure 12. Two bidentate and four tridentate coordination modes are visible for the borohydrides.

DOI: 10.1021/acs.inorgchem.6b00931
Inorg. Chem. 2016, 55, 7090−7097

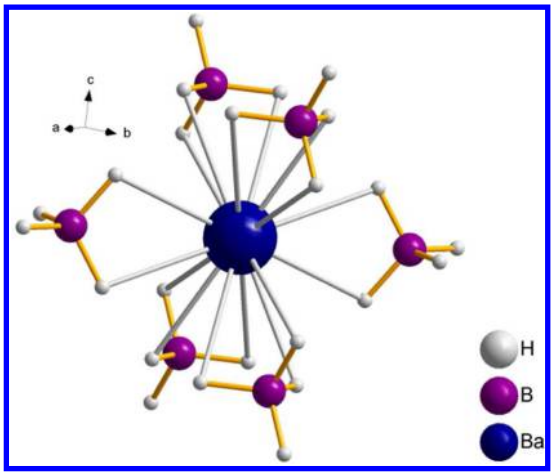

Figure 12. Coordination of borohydrides to Ba in the *Pnnm* polymorph ($CaCl_2$ structure type) of $Ba(BH_4)_2$.

Optimized hydrogen positions allow also for a discussion of H−H intermolecular contacts between neighboring borohydrides. It has been shown that these contacts are at the origin of lowering the crystal symmetry of metal borohydrides from what is expected in simple ionic packing.[66] In the *Pnnm* polymorph of $Ba(BH_4)_2$ the shortest intermolecular H−H contacts of 2.45 Å exist between two straight octahedral chains running along the *c*-axis direction (Figure 13). They form a regular tetrahedron.

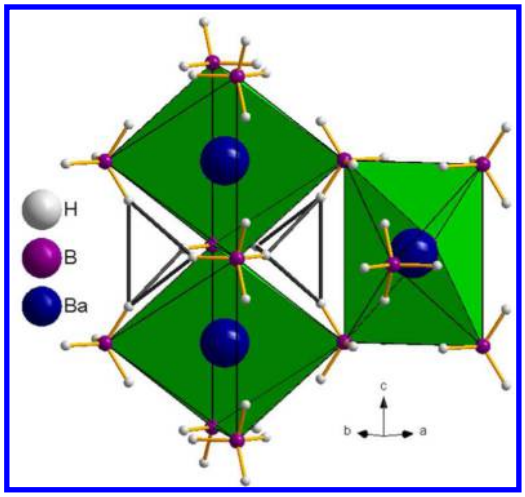

Figure 13. Shortest intermolecular H−H contacts of 2.45 Å (in dark gray) in the *Pnnm* polymorph ($CaCl_2$ structure type) of $Ba(BH_4)_2$.

CONCLUSIONS

Two alkali metals (Sr and Ba) and one bivalent rare earth (Eu) crystallize in structures derived from known structure types based on hcp packing of anions (rutile and α-PbO_2 types) and on simple cubic packing of anions (ccp packing of cations) as in the CaF_2 type and its derivative *ht*-ZrO_2 type. The cation coordination number increases from 6 to 8 with the temperature for all three cations.

The synthesis of halide free metal borohydride is reported. Halide free compounds show higher thermal stability than previously studied samples from chloride based synthesis. The thermal decomposition route of all three borohydrides is rather complex involving unidentified phases, but leads to $M_2(BH_4)H_3$ (M = Sr and Eu), a first compound containing hydride in two anions, as a simple hydride and as a complex borohydride. It is likely that other compounds in the family of $M_2(BH_4)H_3$ can be prepared and studied to see to what extent their formation could take place during the dehydrogenation reaction or whether they can be reversibly converted back to $M(BH_4)_2$. This work is under investigation in our lab.

Stable homopolar H−H intermolecular contacts are of 2.45 Å length as obtained from DFT optimization of $CaCl_2$ (rutile like) type $Ba(BH_4)_2$ polymorph.

ASSOCIATED CONTENT

Supporting Information

The Supporting Information is available free of charge on the ACS Publications website at DOI: 10.1021/acs.inorgchem.6b00931.

Alternate synthesis methods, powder diffraction patterns, Rietveld plots, IR as a function of temperature for $M(BH_4)_2$ (M = Eu, Sr, Ba), CIE color space for $Eu(BH_4)_2$, and table for IR active modes in *Pnnm* structural model of $Ba(BH_4)_2$ (PDF)

Crystallographic details in CIF format (ZIP)

AUTHOR INFORMATION

Corresponding Authors

*E-mail: radovan.cerny@unige.ch.

*E-mail: hans-rudolf.hagemann@unige.ch. Phone +41 22 379 6539(6450). Fax +41 22 379 6103, (6108).

Author Contributions

M.S. and E.D. have contributed equally to this work.

Notes

The authors declare no competing financial interest.

ACKNOWLEDGMENTS

This work is supported by the Swiss National Science Foundation. The authors thank Dr H. Kohlmann for providing the EuH_2 and V. D'Anna for the GF calculations.

REFERENCES

(1) Schlapbach, L.; Zuettel, A. *Nature* **2001**, *414*, 353−358.
(2) David, W. I. F. *Faraday Discuss.* **2011**, *151*, 399−414.
(3) Nickels, E. A.; Jones, M. O.; David, W. I. F.; Johnson, S. R.; Lowton, R. L.; Sommariva, M.; Edwards, P. P. *Angew. Chem., Int. Ed.* **2008**, *47*, 2817−2819.
(4) de Jongh, P. E.; Adelhelm, P. *ChemSusChem* **2010**, *3*, 1332−1348.
(5) Matsuo, M.; Nakamori, Y.; Orimo, S.-i.; Maekawa, H.; Takamura, H. *Appl. Phys. Lett.* **2007**, *91*, 224103-1−224103-3.
(6) Ley, M. B.; Ravnsbaek, D. B.; Filinchuk, Y.; Lee, Y.-S.; Janot, R.; Cho, Y. W.; Skibsted, J.; Jensen, T. R. *Chem. Mater.* **2012**, *24*, 1654−1663.
(7) Sadikin, Y.; Brighi, M.; Schouwink, P.; Černý, R. *Adv. Energy Mater.* **2015**, *5*, n/a.
(8) Schouwink, P.; Ley, M. B.; Tissot, A.; Hagemann, H.; Jensen, T. R.; Smrcok, L.; Černý, R. *Nat. Commun.* **2014**, *5*, 5706.
(9) Schouwink, P.; Didelot, E.; Lee, Y.-S.; Mazet, T.; Černý, R. *J. Alloys Compd.* **2016**, *664*, 378−384.
(10) Brighi, M.; Schouwink, P.; Sadikin, Y.; Černý, R. *J. Alloys Compd.* **2016**, *662*, 388−395.
(11) Lee, J. Y.; Lee, Y.-S.; Suh, J.-Y.; Shim, J.-H.; Cho, Y. W. *J. Alloys Compd.* **2010**, *506*, 721−727.
(12) Mosegaard, L.; Moller, B.; Jorgensen, J.-E.; Filinchuk, Y.; Cerenius, Y.; Hanson, J. C.; Dimasi, E.; Besenbacher, F.; Jensen, T. R. *J. Phys. Chem. C* **2008**, *112*, 1299−1303.

DOI: 10.1021/acs.inorgchem.6b00931
Inorg. Chem. 2016, 55, 7090−7097

(13) Černý, R.; Ravnsbæk, D. B.; Severa, G.; Filinchuk, Y.; D'Anna, V.; Hagemann, H.; Haase, D.; Skibsted, J.; Jensen, C. M.; Jensen, T. R. *J. Phys. Chem. C* **2010**, *114*, 19540−19549.
(14) Ravnsbaek, D. B.; Rude, L. H.; Jensen, T. R. *J. Solid State Chem.* **2011**, *184*, 1858−1866.
(15) Olsen, J. E.; Sorby, M. H.; Hauback, B. C. *J. Alloys Compd.* **2011**, *509*, L228−L231.
(16) Grove, H.; Rude, L. H.; Jensen, T. R.; Corno, M.; Ugliengo, P.; Baricco, M.; Sorby, M. H.; Hauback, B. C. *RSC Adv.* **2014**, *4*, 4736−4742.
(17) Rude, L. H.; Nielsen, T. K.; Ravnsbaek, D. B.; Boesenberg, U.; Ley, M. B.; Richter, B.; Arnbjerg, L. M.; Dornheim, M.; Filinchuk, Y.; Besenbacher, F.; Jensen, T. R. *Phys. Status Solidi A* **2011**, *208*, 1754−1773.
(18) Sharma, M.; Sethio, D.; D'Anna, V.; Hagemann, H. *Int. J. Hydrogen Energy* **2015**, *40*, 12721−12726.
(19) Corno, M.; Pinatel, E.; Ugliengo, P.; Baricco, M. *J. Alloys Compd.* **2011**, *509*, S679−S683.
(20) Yin, L.; Wang, P.; Fang, Z.; Cheng, H. *Chem. Phys. Lett.* **2008**, *450*, 318−321.
(21) Hagemann, H.; Černý, R. *Dalton Trans.* **2010**, *39*, 6006−6012.
(22) Huot, J.; Ravnsbaek, D. B.; Zhang, J.; Cuevas, F.; Latroche, M.; Jensen, T. R. *Prog. Mater. Sci.* **2013**, *58*, 30−75.
(23) Jaron, T.; Orlowski, P. A.; Wegner, W.; Fijalkowski, K. J.; Leszczynski, P. J.; Grochala, W. *Angew. Chem., Int. Ed.* **2015**, *54*, 1236−1239.
(24) Hagemann, H.; Longhini, M.; Kaminski, J. W.; Wesolowski, T. A.; Černý, R.; Penin, N.; Sørby, M. H.; Hauback, B. C.; Severa, G.; Jensen, C. M. *J. Phys. Chem. A* **2008**, *112*, 7551−7555.
(25) Ravnsbaek, D.; Filinchuk, Y.; Cerenius, Y.; Jakobsen, H. J.; Besenbacher, F.; Skibsted, J.; Jensen, T. R. *Angew. Chem., Int. Ed.* **2009**, *48*, 6659−6663.
(26) Ravnsbaek, D. B.; Soerensen, L. H.; Filinchuk, Y.; Reed, D.; Book, D.; Jakobsen, H. J.; Besenbacher, F.; Skibsted, J.; Jensen, T. R. *Eur. J. Inorg. Chem.* **2010**, *2010*, 1608−1612.
(27) Arnbjerg, L. M.; Ravnsbaek, D. B.; Filinchuk, Y.; Vang, R. T.; Cerenius, Y.; Besenbacher, F.; Jorgensen, J.-E.; Jakobsen, H. J.; Jensen, T. R. *Chem. Mater.* **2009**, *21*, 5772−5782.
(28) Černý, R.; Severa, G.; Ravnsbæk, D. B.; Filinchuk, Y.; D'Anna, V.; Hagemann, H.; Haase, D.; Jensen, C. M.; Jensen, T. R. *J. Phys. Chem. C* **2010**, *114*, 1357−1364.
(29) Brown, H. C.; Choi, Y. M.; Narasimhan, S. *Inorg. Chem.* **1982**, *21*, 3657−61.
(30) Soloveichik, G. L.; Andrus, M.; Gao, Y.; Zhao, J. C.; Kniajanski, S. *Int. J. Hydrogen Energy* **2009**, *34*, 2144−2152.
(31) Tumanov, N. A.; Safin, D. A.; Richter, B.; Lodziana, Z.; Jensen, T. R.; Garcia, Y.; Filinchuk, Y. *Dalton Trans.* **2015**, *44*, 6571−6580.
(32) Richter, B.; Ravnsbaek, D. B.; Tumanov, N.; Filinchuk, Y.; Jensen, T. R. *Dalton Trans.* **2015**, *44*, 3988−3996.
(33) Lascola, R.; Knight, D. A.; Mohtadi, R.; Sivasubramanian, P.; Zidan, R. *Int. J. Hydrogen Energy* **2013**, *38*, 13368−13380.
(34) Olsen, J. E.; Frommen, C.; Jensen, T. R.; Riktor, M. D.; Sorby, M. H.; Hauback, B. C. *RSC Adv.* **2014**, *4*, 1570−1582.
(35) Humphries, T. D.; Ley, M. B.; Frommen, C.; Munroe, K. T.; Jensen, T. R.; Hauback, B. C. *J. Mater. Chem. A* **2015**, *3*, 691−698.
(36) Ravnsbaek, D. B.; Nickels, E. A.; Černý, R.; Olesen, C. H.; David, W. I. F.; Edwards, P. P.; Filinchuk, Y.; Jensen, T. R. *Inorg. Chem.* **2013**, *52*, 10877−10885.
(37) Ravnsbaek, D. B. Ph.D. Thesis, 2011.
(38) Chlopek, K.; Frommen, C.; Leon, A.; Zabara, O.; Fichtner, M. *J. Mater. Chem.* **2007**, *17*, 3496−3503.
(39) Hammersley, A. P.; Svensson, S. O.; Hanfland, M.; Fitch, A. N.; Häusermann, D. *High Pressure Res.* **1996**, *14*, 235−248.
(40) Černý, R.; Filinchuk, Y. *Z. Kristallogr. - Cryst. Mater.* **2011**, *226*, 882−891.
(41) Favre-Nicolin, V.; Černý, R. *J. Appl. Crystallogr.* **2002**, *35*, 734−743.
(42) Rodriguez-Carvajal, J. *Phys. B (Amsterdam, Neth.)* **1993**, *192*, 55−69.
(43) Spek, L. A. *PLATON*; 2006.
(44) Hohenberg, P.; Kohn, W. *Phys. Rev.* **1964**, *136*, B864−B871.
(45) Kohn, W.; Sham, L. J. *Phys. Rev.* **1965**, *140*, A1133−A1138.
(46) Perdew, J. P.; Burke, K.; Ernzerhof, M. *Phys. Rev. Lett.* **1996**, *77*, 3865−3868.
(47) Giannozzi, P.; Baroni, S.; Bonini, N.; Calandra, M.; Car, R.; Cavazzoni, C.; Ceresoli, D.; Chiarotti, G. L.; Cococcioni, M.; Dabo, I.; Dal Corso, A.; de Gironcoli, S.; Fabris, S.; Fratesi, G.; Gebauer, R.; Gerstmann, U.; Gougoussis, C.; Kokalj, A.; Lazzeri, M.; Martin-Samos, L.; Marzari, N.; Mauri, F.; Mazzarello, R.; Paolini, S.; Pasquarello, A.; Paulatto, L.; Sbraccia, C.; Scandolo, S.; Sclauzero, G.; Seitsonen, A. P.; Smogunov, A.; Umari, P.; Wentzcovitch, R. M. *J. Phys.: Condens. Matter* **2009**, *21*, 395502.
(48) Baroni, S.; de Gironcoli, S.; Dal Corso, A.; Giannozzi, P. *Rev. Mod. Phys.* **2001**, *73*, 515−562.
(49) Vanderbilt, D. *Phys. Rev. B: Condens. Matter Mater. Phys.* **1990**, *41*, 7892−7895.
(50) Monkhorst, H. J.; Pack, J. D. *Phys. Rev. B* **1976**, *13*, 5188−5192.
(51) Perdew, J. P.; Wang, Y. *Phys. Rev. B: Condens. Matter Mater. Phys.* **1992**, *45*, 13244−13249.
(52) Slater, J. C. *Phys. Rev.* **1951**, *81*, 385−390.
(53) Troullier, N.; Martins, J. L. *Phys. Rev. B: Condens. Matter Mater. Phys.* **1991**, *43*, 1993−2006.
(54) D'Anna, V.; Spyratou, A.; Sharma, M.; Hagemann, H. *Spectrochim. Acta, Part A* **2014**, *128*, 902−906.
(55) Dorenbos, P. *J. Phys.: Condens. Matter* **2003**, *15*, 2645−2665.
(56) Shannon, R. D. *Acta Crystallogr., Sect. A: Cryst. Phys., Diffr., Theor. Gen. Crystallogr.* **1976**, *A32*, 751−767.
(57) Rude, L. H.; Filinchuk, Y.; Sorby, M. H.; Hauback, B. C.; Besenbacher, F.; Jensen, T. R. *J. Phys. Chem. C* **2011**, *115*, 7768−7777.
(58) Carbonnière, P.; Hagemann, H. *J. Phys. Chem. A* **2006**, *110*, 9927−9933.
(59) D'Anna, V.; Lawson Daku, L. M.; Hagemann, H. *J. Phys. Chem. C* **2015**, *119*, 21868−21874.
(60) Hyde, B. G.; Andersson, S. *Inorganic Crystal Structures*; John Wiley and Sons, 1989; p 430.
(61) Reckeweg, O.; DiSalvo, F. J. *Z. Naturforsch., B: J. Chem. Sci.* **2010**, *65*, 493−498.
(62) Reckeweg, O.; DiSalvo, F. J. *Z. Naturforsch., B: J. Chem. Sci.* **2011**, *66*, 21−26.
(63) Reckeweg, O.; DiSalvo, F. J. *Z. Naturforsch., B: J. Chem. Sci.* **2011**, *66*, 1087−1091.
(64) Reckeweg, O.; Molstad, J. C.; Levy, S.; DiSalvo, F. *Z. Naturforsch., B: J. Chem. Sci.* **2007**, *62*, 23−27.
(65) Grund, I.; Schuster, H. U.; Müller, P. *Z. Z. Anorg. Allg. Chem.* **1984**, *515*, 151−158.
(66) Černý, R.; Schouwink, P. *Acta Crystallogr., Sect. B: Struct. Sci., Cryst. Eng. Mater.* **2015**, *71*, 619−640.

DOI: 10.1021/acs.inorgchem.6b00931
Inorg. Chem. 2016, 55, 7090−7097